Macromolecules

pubs.acs.org/Macromolecules

Article

Consequences of Molecular Architecture on the Supramolecular Assembly of Discrete Block Co-oligomers

Brigitte A. G. Lamers,[⊥] Joost J. B. van der Tol,[⊥] Kasper M. Vonk, Bas F. M. de Waal, Anja R. A. Palmans, E. W. Meijer, and Ghislaine Vantomme*

Cite This: *Macromolecules* 2020, 53, 10289−10298

Read Online

ACCESS | Metrics & More | Article Recommendations | Supporting Information

ABSTRACT: Supramolecular block copolymers composed of discrete blocks have promising properties for nanotechnology resulting from their ability to combine well-defined morphologies with good bulk material properties. Here, we present the impact of a well-defined siloxane block in either the main-chain or present as pendant grafts on the properties of supramolecular block copolymers that form ordered nanostructures with sub-5 nm domains. For this, two types of supramolecular block copolymers were synthesized based on the ureidopyrimidinone−urethane (UPy-UT) motif. In the first, oligodimethylsiloxanes (*o*DMS) of discrete length were end-capped with the UPy-UT motif, affording main-chain **UPy-UT-Si$_n$**. In the second, the UPy-UT motif was grafted with discrete *o*DMS affording grafted **UPy-UT-*g*-Si$_7$**. For the two systems, the compositions are similar; only the molecular architecture differs. In both cases, crystallization of the UPy-UT block is in synergy with phase segregation of the *o*DMS, resulting in the formation of lamellar morphologies. The grafted **UPy-UT-*g*-Si$_7$** can form long-range ordered lamellae, resulting in the formation of micrometer-sized 2D sheets of supramolecular polymers which show brittle properties. In contrast, **UPy-UT-Si$_n$** forms a ductile material. As the compositions of both BCOs are similar, the differences in morphology and mechanical properties are a direct consequence of the molecular architecture. These results showcase how molecular design of the building block capable of forming block copolymers translates into controlled nanostructures and material properties as a result of the supramolecular nature of the interactions.

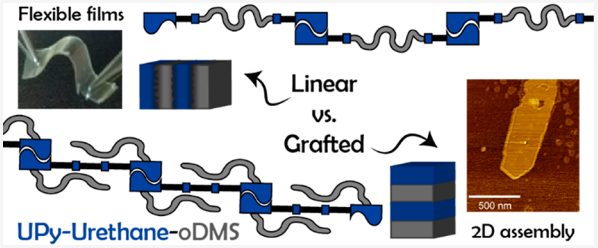

INTRODUCTION

Approaching the fundamental limits in classical lithography techniques has sparked a search for alternative innovations in semiconductor and optoelectronics technology. Examples of exciting developments also include 2D nanomaterials[1−3] that are supramolecularly assembled for adaptive materials, flexible displays and devices, or electronic skins.[4,5] A characteristic of all these technologies is that they require materials with highly organized nanostructures, while at the same time these materials need to show good mechanical properties. The combination of these properties in one material, however, is rarely obtained.[6] Therefore, to catalyze the development of these technologies, tough materials that combine mechanical properties with precise nanoscale organization are required.

One of the most widely explored methods to control nanoscale architectures is the assembly of block copolymers (BCPs) into various microphase-segregated morphologies.[7−11] The domain (i.e., feature) sizes and phase boundaries are determined by the polymer length (N), composition, molecular weight distribution ($Đ$), and the Flory−Huggins interaction parameter (χ).[12] The recent interest in morphologies with sub-10 nm features has resulted in extensive research to minimize N and maximize the immiscibility (χ).[13] One strategy includes shifting the phase boundaries by varying the molecular architecture of BCPs.[14−16] For this, the influence of branching BCPs on the morphology has been explored by, for example, grafted,[17] H-shaped,[18,19] Y-shaped,[20,21] and star polymers.[22−24] Nevertheless, the resolution of the nanoscale morphologies has remained suboptimal due to the dispersity of the BCPs, resulting in a poorly defined interface between the two blocks.

To overcome the challenges in obtaining sharp, defined interface boundaries, another strategy toward perfectly organized sub-10 nm structures was recently exploited, focusing on the absence of dispersity in BCPs. For this, linear block co-oligomers (BCOs), with one block consisting of oligodimethylsiloxane (*o*DMS) of discrete length ($Đ$ = 1), were developed.[25−27] The discrete design, high immiscibility of the *o*DMS block with many other oligomeric blocks, and low N contributed to improve the resolution at the domain interface while accessing sub-10 nm feature sizes. The additional

Received: September 30, 2020
Revised: October 27, 2020
Published: November 11, 2020

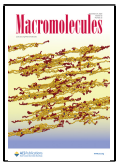

https://dx.doi.org/10.1021/acs.macromol.0c02237
Macromolecules 2020, 53, 10289−10298

Scheme 1. Molecular Structures of UPy-Si$_n$ and Bz-UPy-Si$_n$,[26] Bz-UPy-UT-Si$_n$, UPy-UT-Si$_n$, Bz-UPy-UT-*g*-Si$_7$, and UPy-UT-*g*-Si$_7$

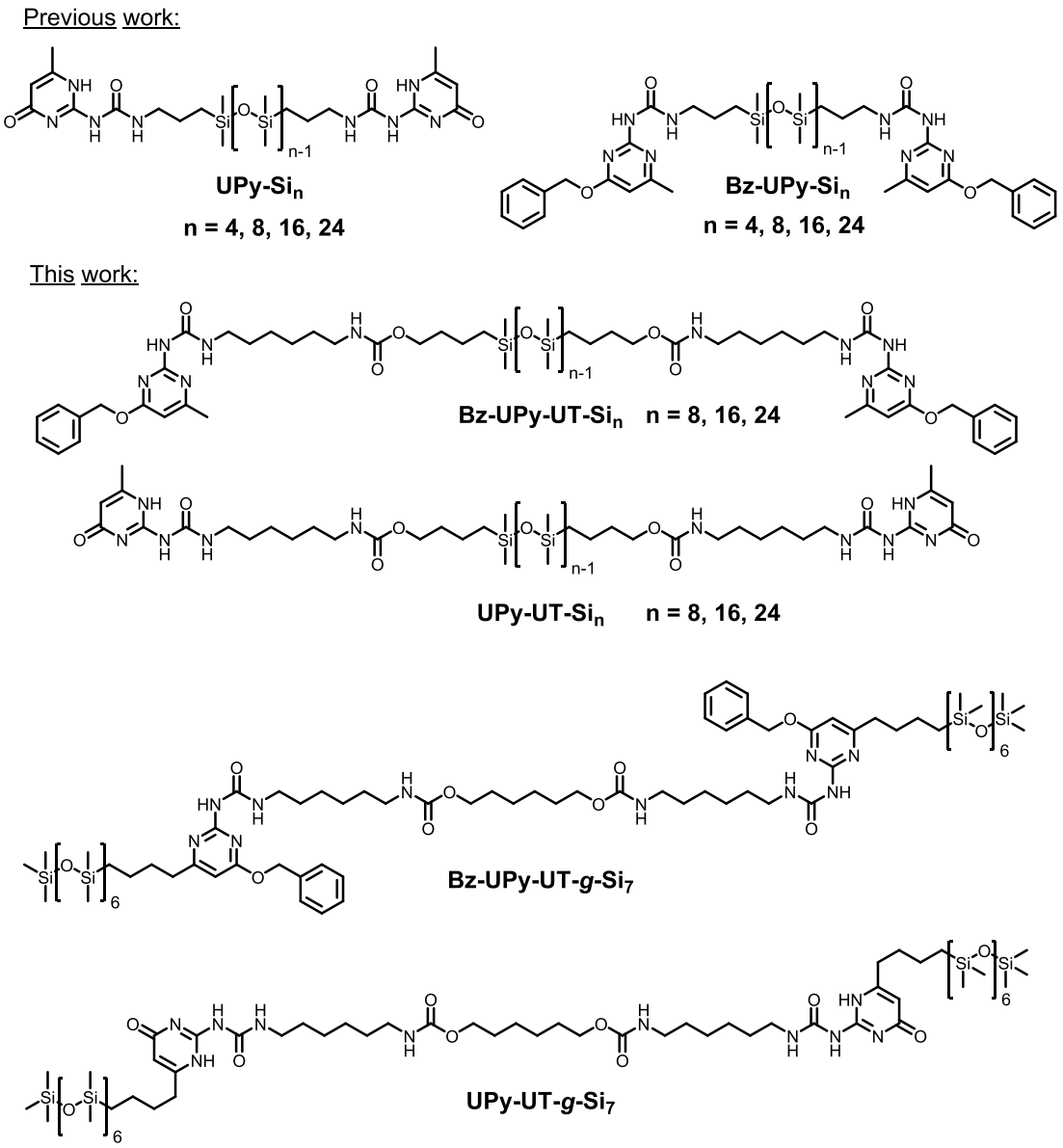

introduction of a crystalline block enhanced the long-range order further due to sharpening of the interface between the blocks.[28−30] Crystallization drives the assembly and resulted in a preferential formation of lamellar nanostructures.[31,32] Moreover, because of the liquid-crystalline properties of these semicrystalline materials, feature sizes down to 2.2 nm were accessed.[33] Hence, these amorphous−crystalline, discrete BCOs are great candidates for 2D materials because of their defined nanostructure. However, as a result of their short BCO chain length, these materials are typically brittle and lack the mechanical properties required for many integrated applications.

One way to introduce toughness in the materials composed of defined, short building blocks are supramolecular interactions, extending the short blocks to form long, main-chain supramolecular BCPs.[34] Such telechelic building blocks are known to induce thermoplastic or elastic properties resulting from entanglements and physical cross-links of the supramolecular BCPs.[35−39] Ureidopyrimidinone (UPy) is a promising supramolecular motif to form tough materials due to the strong, quadruple hydrogen bonding.[40] In the past, we prepared semicrystalline UPy-based supramolecular polymers by the incorporation of urethane functionalities adjacent to the UPy, which gives rise to lateral stacking of the hydrogen bonding moieties.[41−43] However, for these materials, the linkers between the supramolecular moieties possessed a molar mass dispersity, which resulted in the loss of nanoscale organization.

Despite these promising results, design principles to form semicrystalline materials with highly ordered nanostructures and good mechanical properties are still lacking. We envision that, ultimately, a combination of supramolecular motifs and discrete *o*DMS blocks will allow the marriage of bulk and nanoscale properties. We thus set out to explore the assembly processes of amorphous−crystalline supramolecular BCPs and gain insight into the structure−property relationship of the molecular designed materials.

https://dx.doi.org/10.1021/acs.macromol.0c02237
Macromolecules 2020, 53, 10289−10298

Table 1. Thermal and Morphological Characterization of Grafted and Linear (Bz)-UPy-UT-Si$_n$ Block Co-oligomers Obtained by DSC and X-ray Scattering Analysis

entry	BCO[a]	M_n[b] [Da]	f_{Si}[c]	T_m[d] [°C]	ΔH_{fus}[d] [kJ mol^{-1}]	T_{ODT}[d] [°C]	T_{DOT}[e] [°C]	T_c[e] [°C]	d_{LAM}[f] [nm]
1	**UPy-UT-Si$_8$**	1310	0.57	70.9	8.6	154.6	126.4	2.9	4.3
2	**UPy-UT-Si$_{16}$**	1903	0.73	60.5	15.1	164.6	144.1	21.2	5.0
3	**UPy-UT-Si$_{24}$**	2497	0.80	52.2	15.5	142.3	123.5	11.0	5.9
4	**Bz-UPy-UT-Si$_8$**	1490	0.51	58.7[g]	45.3	n.o.	n.o.	n.o.	3.5
5	**Bz-UPy-UT-Si$_{16}$**	2084	0.67	59.4[g] (27.9)[h]	61.7 (19.9)[h]	n.o.	n.o.	n.o.	4.8
6	**Bz-UPy-UT-Si$_{24}$**	2677	0.76	39.6[g]	28.5	n.o.	n.o.	n.o.	6.0
7	**UPy-UT-*g*-Si$_7$**	1823	0.73	103.2	23.4	n.o.	n.o.	21.1	3.7
8	**Bz-UPy-UT-*g*-Si$_7$**	2003	0.68	n.o.	n.o.	94.7	n.d.	n.o.	3.5

[a]Block co-oligomers (BCO) as depicted in Scheme 1. [b]Calculated value of M_n. [c]Volume fraction of the siloxane block, calculated using bulk densities for PDMS (0.95 g mL^{-1})[25] and UPy (1.33 g mL^{-1}).[48] [d]Melt transition temperature (T_m) with corresponding enthalpy of fusion per mole BCO (ΔH_{fus}) and order−disorder transition temperature (T_{ODT}) determined with DSC using a heating rate of 10 and 5 K min^{-1} for the protected and deprotected BCOs, respectively. [e]Disorder−order transition temperature (T_{DOT}) and crystallization transition temperature (T_c) determined with DSC using a cooling rate of 5 K min^{-1}. [f]Lamellar domain spacing of the crystalline phase examined with MAXS at room temperature and calculated from $d = 2\pi/q^*$. [g]Transition only observed in the first heating run during the DSC measurement. [h]Melting temperature and enthalpy of fusion between brackets measured during the second heating cycle of the DSC measurement; n.o. = not observed; n.d. = not determined.

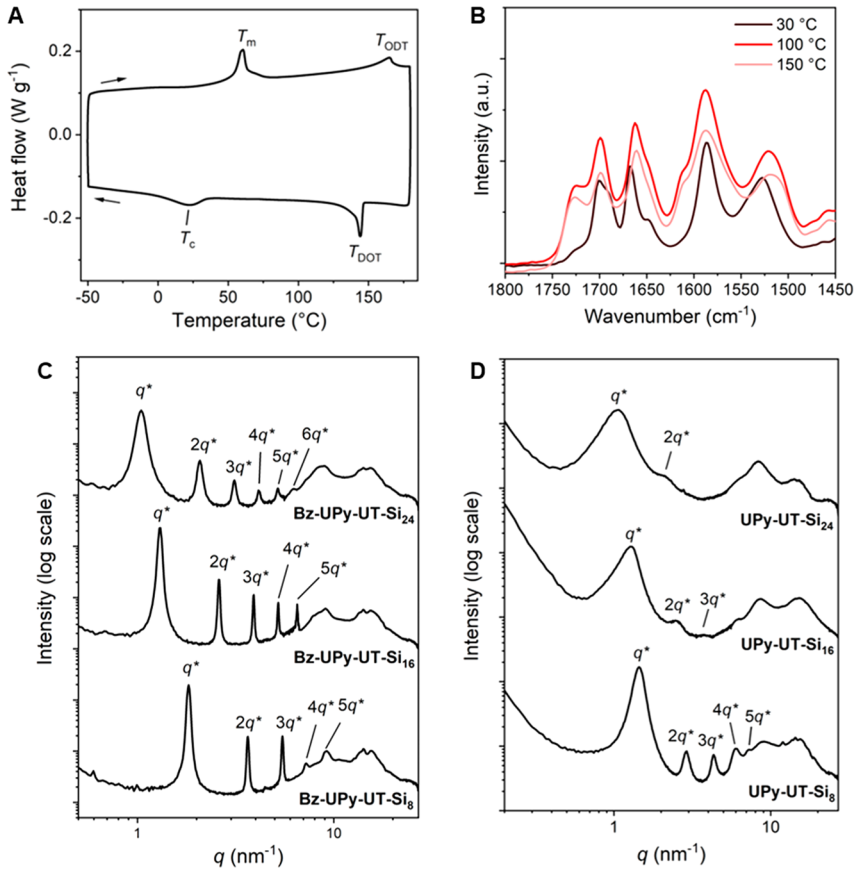

Figure 1. (A) DSC trace of **UPy-UT-Si$_{16}$** (second heating and cooling run). Endothermic heat flows have a positive value. A temperature ramp of 5 K min^{-1} was used. (B) FT-IR spectra of **UPy-UT-Si$_{16}$** at elevated temperatures, measured upon heating. (C) 1D transmission scattering profiles of **Bz-UPy-UT-Si$_n$** and (D) of **UPy-UT-Si$_n$** both at room temperature. The MAXS and WAXS samples were heated to the isotropic state, cooled to room temperature (5 K min^{-1}), and measured a month after equilibration at room temperature.

Here, we report on the consequences of molecular architecture on the bulk properties of supramolecular assemblies of discrete, amorphous−crystalline block co-oligomers. Thereby the influence of crystallization and architecture on nanoscale organization and bulk properties is studied, as is widely done for classical BCPs.[44−47] To this end, we synthesized and assembled a set of UPy−urethane (UPy-UT) functionalized discrete siloxane oligomers to obtain semicrystalline supramolecular BCPs with two different molecular architectures (Scheme 1). Hence, a UPy-UT-*o*DMS alternating main-chain supramolecular BCP and a UPy-UT main-chain supramolecular polymer grafted with *o*DMS are formed. With this, we expand our understanding of the effect of architecture and block dispersity of supramolecular, semicrystalline BCPs and their influence on the nanostructure and material properties.

https://dx.doi.org/10.1021/acs.macromol.0c02237
Macromolecules 2020, 53, 10289−10298

RESULTS AND DISCUSSION

Ureidopyrimidinone−Urethane−Oligodimethylsiloxane Block Co-oligomer Synthesis. We synthesized two architectures of ureidopyrimidinone−urethane (UPy-UT) BCOs with discrete, oligodimethylsiloxane (*o*DMS) as the soft, amorphous block and UPy-UT representing the hard, supramolecular assembling block. Inspired by our previous work on UPy end-functionalized siloxanes (Scheme 1), the linear architecture was synthesized from *o*DMS dihydrides with a length of 8, 16, or 24 repeating units (denoted as Si_8, Si_{16}, or Si_{24}, respectively).[33] The UPy-UT block was obtained by monosubstitution of 1,6-hexyldiisocyanate with methylisocytosine followed by reaction with an olefin-terminated alcohol (Scheme S1). Benzyl protection of the carbonyl-UPy was performed to selectively react the olefin-terminated UPy-UT to the *o*DMS dihydrides through platinum-catalyzed hydrosilylation. This resulted in three end-functionalized oligomers in 30−70% yields denoted as **Bz-UPy-UT-Si$_n$**, with n the number of siloxane repeating units (Scheme 1). The benzyl-protected UPy-UT BCOs were obtained as white, crystalline powders. Subsequent removal of the benzyl group by catalytic hydrogenation afforded **UPy-UT-Si$_n$** BCOs (27−52% yield) as transparent plastics. The UPy-UT grafted with *o*DMS was synthesized from ethyl acetoacetate to obtain butenylisocytosine (Scheme S2). Similar to the linear architecture, the 1,6-hexyldiisocyanate was monosubstituted with the isocytosine, followed by a reaction of the UPy-isocyanate with a diol to obtain the UPy-UT block. After benzyl protection, the olefin-terminated 6-position of the UPy was reacted with *o*DMS_7-monohydride completing the benzyl-protected grafted architecture in 48% yield, denoted as **Bz-UPy-UT-*g*-Si$_7$** (Scheme 1). In contrast to the linear benzyl-protected analogues that were obtained as crystalline solids, **Bz-UPy-UT-*g*-Si$_7$** was obtained as a viscous liquid. Removal of the benzyl group resulted in **UPy-UT-*g*-Si$_7$** (52% yield), a brittle solid.

The volume fraction of siloxane per end-functionalized oligomer is similar for the grafted **UPy-UT-*g*-Si$_7$** and the linear **UPy-UT-Si$_{16}$** (Table 1). This allows us to compare between the linear and grafted architectures and their effect on the BCO thermal, morphological, and mechanical properties. First, the linear BCOs are discussed, and we focus on the effect of the *o*DMS volume fraction on the BCO properties. We also compare the properties and morphologies of the linear **UPy-UT-Si$_n$** and **Bz-UPy-UT-Si$_n$** BCOs to the previously reported **UPy-Si$_n$** and **Bz-UPy-Si$_n$** as the design and siloxane volume fractions are very similar.[33] In the second part, we focus on the characterization of **UPy-UT-*g*-Si$_7$** and compare the properties to those of **UPy-UT-Si$_{16}$**.

Crystallization-Driven Assembly of Linear UPy-UT-Si$_n$ and Bz-UPy-UT-Si$_n$ into Lamellar Nanostructures. We assume that complementary to UPy dimerization, urethane hydrogen bonding introduces crystallinity in the BCOs by lateral stacking of the UPy dimers, as known from previous studies.[42] Therefore, the thermal transitions of **UPy-UT-Si$_n$** and **Bz-UPy-UT-Si$_n$** were examined by using DSC. The thermograms of the linear **UPy-UT-Si$_n$** BCOs show a major endothermic transition and a second, much weaker endotherm upon heating (Figure 1A and Figure S9). This first transition represents melting of the crystalline domains with an enthalpic energy of 8.6−15.5 kJ mol^{-1} (Table 1, entries 1−3). The melting temperatures (T_m) range from 70.9 to 52.2 °C going from a siloxane linker of 8 to 24 repeating units, respectively. Fourier transform infrared (FT-IR) spectroscopy above T_m indicates the hydrogen-bond dissociation of the urethanes by the appearance of the peak at 1726 cm^{-1} indicative of free C=O (Figure 1B and Figure S10). Hence, melting of the material is a result of the dissociation of the urethane bonds. We assign the weaker endothermic transition at higher temperatures (150 °C) to an order−disorder transition (T_{ODT}) from an amorphous, phase-segregated state to the isotropic state (*vide infra*). Upon cooling, organization into the amorphous, phase-segregated state occurs first (T_{DOT}), followed by crystallization (T_c) at 2.9−21.2 °C.

The first DSC heating run of the linear, benzyl-protected oligomers **Bz-UPy-UT-Si$_n$** showed melting temperatures at lower temperatures in all cases (Figure S11A) compared to the deprotected analogues (Table 1, entries 1−6). However, the enthalpic energy released upon melting was significantly higher for the protected BCOs (28.5−61.7 kJ mol^{-1}). We attribute these differences in enthalpic energy to the efficiency in the molecular packing in the presence of the benzyl group, which will be discussed below. The melt transitions are absent in the second heating run, but a clear glass transition temperature (T_g) at −21 to −35 °C is observed instead (Figure S11A). As the only exception, **Bz-UPy-UT-Si$_{16}$** exhibits a cold crystallization transition during the second heating cycle, followed by a melting transition (Figure S11A). No order−disorder transitions were observed for the protected **Bz-UPy-UT-Si$_n$**.

Medium- and wide-angle X-ray scattering (MAXS and WAXS) at room temperature were conducted to investigate the presence of ordered structures below T_m. The 1D transmission scattering data of the linear **UPy-UT-Si$_n$** and **Bz-UPy-UT-Si$_n$** are shown in Figure 1C,D. A lamellar structure was determined by the presence of a primary scattering peak (q^*) followed by its integer multiples ($2q^*$, $3q^*$, ...) for all linear BCOs. The related domain sizes were calculated and tabulated as d_{LAM} in Table 1. The formation of a lamellar structure irrespective of the siloxane volume fraction indicates that crystallization is the driving force for nanostructure organization. This was confirmed by the appearance of scattering peaks in the wide-angle region (q > 7 nm^{-1}), suggesting crystallization of the UPy-UT moieties. For **UPy-UT-Si$_n$**, the crystallization is governed by the lateral stacking of the UPy dimers supported by the urethane hydrogen bonding as discussed above. No crystallization was observed for the previously reported **UPy-Si$_n$**,[33] and therefore we conclude that the urethane bonds positioned next to a UPy moiety are key to obtain a crystallization-driven assembly. A schematic representation of the crystalline, lamellar nanostructure inferred from the X-ray diffraction results is given in Figure 2A,B. The scattering peaks of **UPy-UT-Si$_n$** are relatively broad (Figure 1D), which becomes more pronounced when the volume fraction of siloxane becomes larger (e.g., for **UPy-UT-Si$_{24}$**). Most likely, this is due to the competition between phase segregation and crystallization, resulting in a more distorted structure. Nevertheless, the discrete design of the linker is crucial to obtain the ordered lamellae as a disperse reference **UPy-UT-Si$_{\sim 20}$** BCO shows significant broadening of the scattering peaks, indicative of broader interfaces between the lamellae (Figure S12). The discrete, benzyl-protected BCOs (**Bz-UPy-UT-Si$_n$**) exhibit sharp scattering peaks in the 1D transmission scattering profiles (Figure 1C). Hence, the lamellae are more ordered, and crystallization of the benzyl-protected BCOs is more favorable than for the **UPy-UT-Si$_n$** due to a more efficient packing of the benzyl-protected UPy-

https://dx.doi.org/10.1021/acs.macromol.0c02237
Macromolecules 2020, 53, 10289−10298

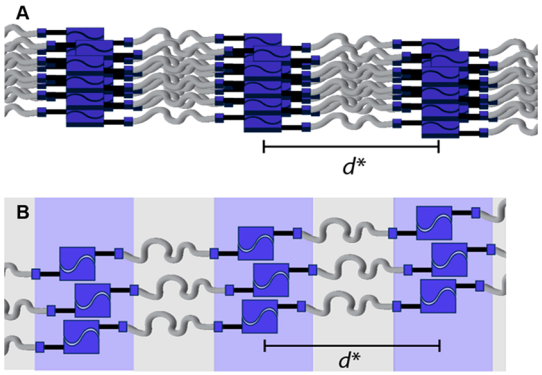

Figure 2. Schematic representation of the (A) side and (B) top view of the **UPy-UT-Si$_{16}$** bulk, crystalline, lamellar morphology at room temperature.

UT. This in accordance with the higher enthalpic energy corresponding to the melting of **Bz-UPy-UT-Si$_n$** compared to the deprotected analogues (*vide supra*). Most likely, the crystalline packing of **Bz-UPy-UT-Si$_n$** is similar to that of the previously reported **Bz-UPy-Si$_n$** in which the crystallization is driven by slipped stacking of phenyl and pyrimidine rings as well as CH···π interactions.[33] The only difference in molecular design is the urethane bond including a C_6 linker of which the combination has a length of ∼0.65 nm. When comparing the domain spacings of **Bz-UPy-UT-Si$_n$** with those of **Bz-UPy-Si$_n$**, we observe a d_{LAM} that is consistently 1.2−1.3 nm higher for the **Bz-UPy-UT-Si$_n$** BCOs for all siloxane lengths. For example, the domain spacing of **Bz-UPy-Si$_8$** is 2.2 nm,[33] and **Bz-UPy-UT-Si$_8$** shows a domain spacing of 3.5 nm (Table 1, entry 4). The difference of 1.3 nm arises from the length of the urethane with C_6 linker that is incorporated twice for **Bz-UPy-UT-Si$_n$**. From these results, we conclude that **Bz-UPy-UT-Si$_n$** and **Bz-UPy-Si$_n$** show a similar packing.

Variable temperature X-ray scattering experiments were conducted to understand the morphological changes revealed by the DSC measurements upon heating and cooling. A selection of 1D MAXS profiles of **UPy-UT-Si$_{16}$**, representative of the morphology changes in the linear analogues, are shown in Figure 3. Upon heating, the profile of **UPy-UT-Si$_{16}$** changes from a broad scattering peak at room temperature to sharp reflection peaks at 60 °C (q_2*) (Figure 3A), indicating a change in the morphology. At this temperature, the crystalline structure melts as a result of urethane dissociation, in accordance with the DSC data and IR spectra. Hence, an amorphous phase-segregated structure is formed above T_m. The sharp scattering reflection peaks at q_2*, $2q_2$*, $3q_2$*, and $4q_2$* reveal the presence of a lamellar, phase-segregated morphology. The urethane and linker are amorphous above T_m (Figure 3C), and therefore a slightly smaller domain spacing (d_2) of 4.9 nm is obtained compared to the domain spacing of the crystalline, lamellar structure (5.0 nm). A low intensity, third principal scattering peak (q_3*) also appears at 60 °C in the scattering profile (Figure 3A). This structure, with a large domain spacing (d_3) of 9.2 nm, most likely originates from defects in the packing. Herein, some UPy-UT moieties could be mixed in the siloxane fraction. Upon cooling, the three different structures are retained due to the low crystallization temperature (21.2 °C) (Figure 3B). Most likely, the broad peak observed at 20 °C before heating is a combination of all three morphologies. Over the course of a month, the morphology slowly evolves back to the initial profile with broad peaks as crystallization takes place. Similar variable temperature scattering profiles were observed for the **UPy-UT-Si$_8$** and **UPy-UT-Si$_{24}$** (Figure S13). The latter forms a hexagonally packed cylindrical, phase-segregated state above T_m due to the larger fraction of siloxane. Hence, when the crystalline domains melt, the morphology follows the BCP phase segregation theory for the linear analogues.

Crystallization-Driven Assembly of Grafted UPy-UT-*g*-Si$_n$ and Bz-UPy-UT-*g*-Si$_n$ into Highly Ordered Lamellar Nanostructures. To evaluate the effect of the molecular architecture of supramolecular, semicrystalline BCPs, the thermal properties and morphology of the grafted **UPy-UT-*g*-Si$_7$** and **Bz-UPy-UT-*g*-Si$_7$** BCOs were examined. We

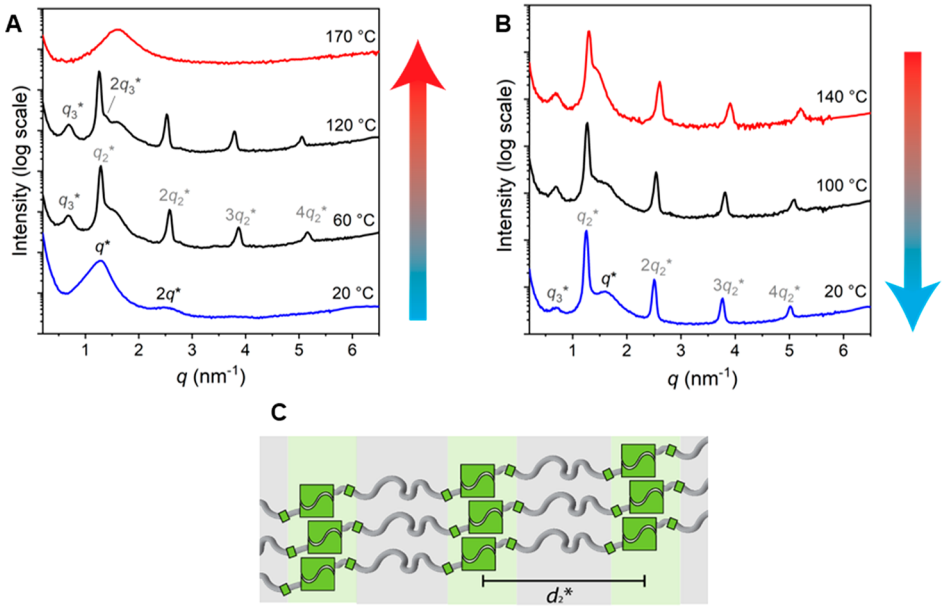

Figure 3. 1D transmission scattering profiles for **UPy-UT-Si$_{16}$** at various temperatures upon (A) heating and (B) cooling. (C) Schematic representation (top view) of the amorphous lamellar phase (q_2).

https://dx.doi.org/10.1021/acs.macromol.0c02237
Macromolecules 2020, 53, 10289−10298

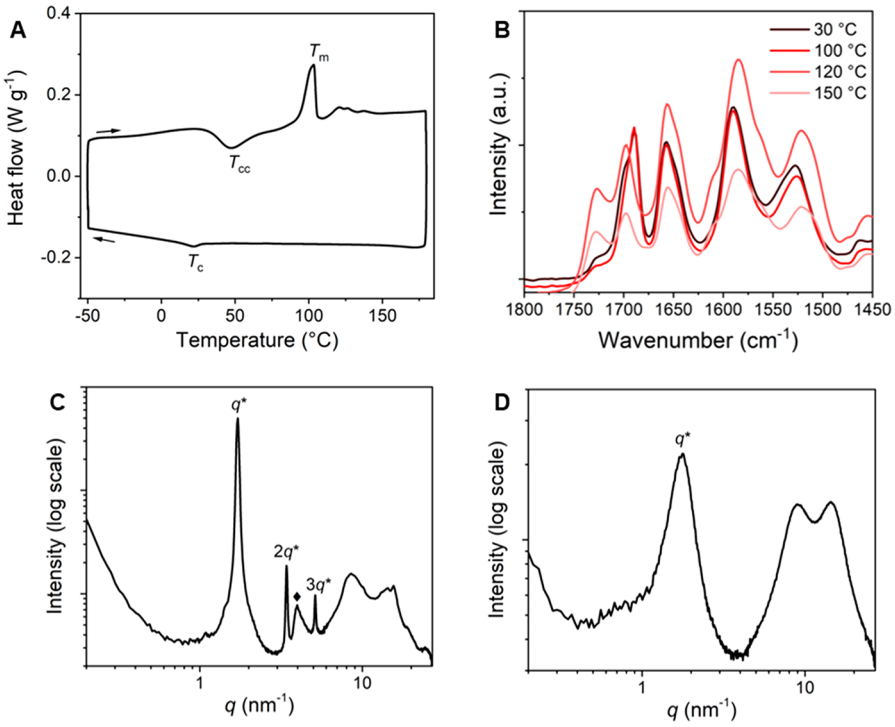

Figure 4. (A) DSC trace of **UPy-UT-*g*-Si$_7$** (second heating and cooling run). Endothermic heat flows have a positive value. A temperature ramp of 5 K min^{-1} was used. (B) FT-IR spectra of **UPy-UT-*g*-Si$_7$** at elevated temperatures, measured upon heating. 1D transmission scattering profiles of (C) **UPy-UT-*g*-Si$_7$** and (D) **Bz-UPy-UT-*g*-Si$_7$** at room temperature. Secondary UPy interaction is indicated with ♦. The MAXS and WAXS samples were heated to the isotropic state, cooled to room temperature (5 K min^{-1}), and measured a month after equilibration at room temperature.

measured DSC of **UPy-UT-*g*-Si$_7$**, and the thermogram shows a cold crystallization transition temperature (T_{cc}) at 47 °C upon heating (Figure 4A). This is followed by a melt transition temperature (T_m) at 103.2 °C. At this temperature, the absorption peak at 1726 cm^{-1} appears in the variable temperature FT-IR spectra, indicating urethane bond dissociation (Figure 4B). Heating to higher temperatures results in a very broad and weak endothermic transition, of which the origin remains unknown. In contrast to the linear analogues, no amorphous, ordered structured is formed above T_m, and therefore we can exclude an order−disorder transition (*vide infra*). The energy corresponding to melting of the crystalline structure is 23.4 kJ mol^{-1}, which is 3 times larger than for the linear analogues. In contrast, the energy corresponding to the isotropization transition of the grafted, benzyl-protected **Bz-UPy-UT-*g*-Si$_7$** is low (ΔH_{fus} < 5 kJ mol^{-1}) compared to **UPy-UT-*g*-Si$_7$** and **Bz-UPy-UT-Si$_n$** (Table 1, entries 4−8).

The 1D transmission scattering data obtained by MAXS and WAXS experiments of **UPy-UT-*g*-Si$_7$** show the presence of a lamellar structure at room temperature indicated by the presence of q* followed by 2q* and 3q* (Figure 4C). Similar to the linear analogues, the lamellar morphology is formed by crystallization-driven assembly of the UPy-UT confirmed by the reflection peaks in the high q region (>10 nm^{-1}). In contrast, no change in morphology of **UPy-UT-*g*-Si$_7$** was observed upon heating or cooling (Figure S14). Only isotropization of the crystalline, lamellar structure was observed at 120 °C, and the lamellar structure re-formed at 50 °C. The domain spacing (d_{LAM}) is 3.7 nm, which is approximately the length of the oligomer. An additional scattering peak at 4 nm^{-1} appeared which is characteristic for secondary UPy interactions resulting in aggregation of the UPy stacks, reported by Appel and co-workers.[50] Hence, this peak represents the interstack interactions with a distance of 1.5 nm. We hypothesized that the UPy moieties can form this interaction as the siloxane fraction is small enough to only fill the small pockets between the layers, indicated in the schematic illustration of the **UPy-UT-*g*-Si$_7$** packing in Figure 5.

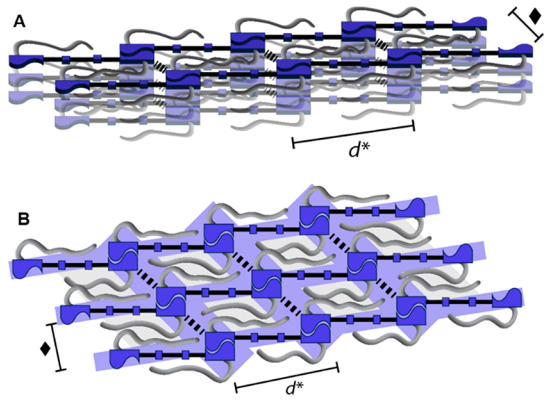

Figure 5. Schematic representation of the (A) side and (B) top view of the **UPy-UT-*g*-Si$_7$** bulk lamellar morphology. The interstack interactions between the UPy dimers are indicated with the dashed lines, and the interstack distance is indicated with ♦.

We strengthened the packing hypothesis with a reference molecule having a siloxane graft that is twice as long (**UPy-UT-*g*-Si$_{15}$**). The **UPy-UT-*g*-Si$_{15}$** transmission scattering profile lacks the additional scattering peak representing the interstack interactions (Figure S15). Therefore, we propose that the layers are pushed away from each other by the larger fraction

https://dx.doi.org/10.1021/acs.macromol.0c02237
Macromolecules 2020, 53, 10289−10298

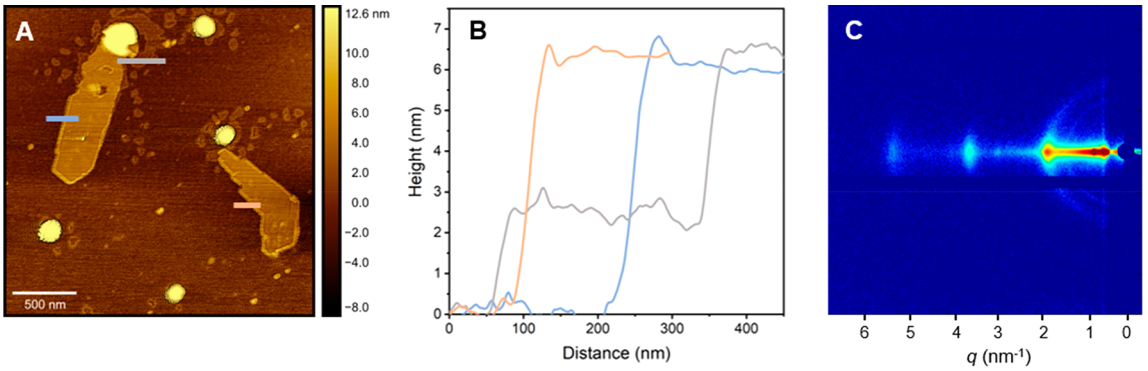

Figure 6. (A) AFM height image and (B) corresponding height profiles of **UPy-UT-*g*-Si$_7$**, 5 μM solution in heptane deposited on silicon wafer. (C) 2D GISAXS pattern of **UPy-UT-*g*-Si$_7$** dropcasted on a silicon wafer.

of siloxane that has to fit in between the UPy-UT layers. In this way, the secondary interactions between the UPy moieties are not able to form.

The packing of the benzyl-protected analogue (**Bz-UPy-UT-*g*-Si$_7$**) is not efficient, resulting in a phase-segregated state with an undefined morphology (Figure 4D). This is in accordance with the DSC data where the enthalpic energy for isotropization is lower for **Bz-UPy-UT-*g*-Si$_7$** compared to **UPy-UT-*g*-Si$_7$** and the linear **Bz-UPy-UT-Si$_n$** (*vide supra*).

Consequences of Molecular Architecture on the Thermal Properties and Nanoscale Morphology. Using the bulk X-ray scattering results in combination with the DSC data and FT-IR spectra (*vide supra*), we can conclude that the urethane bonds positioned next to a UPy moiety are key to obtain a crystallization-driven assembly. In fact, no crystallization was observed for the previously reported **UPy-Si$_n$**.[33] Similarly, we synthesized the **UPy-*g*-Si$_7$** reference molecule, without urethane bonds (Scheme S3). In that case, only a phase-segregated lamellar structure was determined, and no crystalline regions were observed by X-ray scattering experiments (Figure S16). The effect of the molecular architecture on the bulk assembly and crystallization is clearly pointed out by the difference in molecular packing of oligomers **UPy-UT-*g*-Si$_7$** and **UPy-UT-Si$_{16}$** that consist of approximately the same siloxane fraction (f_{Si} = 0.73). **UPy-UT-*g*-Si$_7$** shows sharper scattering peaks at room temperature, indicating a better ordering of the crystalline, lamellar structure (*vide supra*). This was confirmed by the DSC data in which the enthalpy for melting is higher for **UPy-UT-*g*-Si$_7$** than for **UPy-UT-Si$_{16}$** (23.4 and 15.1 kJ mol^{-1}, respectively). This difference in crystallinity is remarkable, and we speculate that it may originate from two types of contributions. First, the additional driving force for aggregation of the UPy dimers as a result of the secondary UPy interactions in **UPy-UT-*g*-Si$_7$** could induce a higher degree of ordering. Second, two UPy-UT moieties connected via a short C$_6$ linker most likely result in a cooperative effect of crystallization of the hard block compared to the linear **UPy-UT-Si$_{16}$** containing an amorphous siloxane linker in-between two UPy-UT units. Therefore, the melting temperature and corresponding enthalpy are higher for the grafted analogue compared to the linear BCO as the larger driving force for crystallization results in larger and better ordered crystalline domains.

2D Nanomaterials of UPy-UT-*g*-Si$_7$. The large driving force for crystallization of **UPy-UT-*g*-Si$_7$** into a lamellar morphology prompted us to investigate the formation of 2D assemblies.[2] Therefore, we conducted atomic force microscopy (AFM) experiments (Figure 6A and Figure S17A,B). The material was dropcasted on a silicon wafer from a dilute heptane solution (5 μM), giving rise to rectangular sheets and small particles. Remarkably, the 2D sheets could be formed without any complex formulation steps, for example, exfoliation and interface- or surface-mediated technics.[49] The sharp edges of the micrometer-sized 2D sheets are indicative for crystallization. A constant height of 6.5 nm along the cross section of the 2D ensemble was measured (Figure 6B).

Grazing-incidence small-angle X-ray scattering (GISAXS) of a more concentrated sample dropcasted on a silicon wafer was conducted. The results confirm the appearance of highly ordered, parallel **UPy-UT-*g*-Si$_7$** layers on the silicon surface, indicated by the bright spots at q^*, $2q^*$, and $3q^*$ on the 2D pattern (Figure 6C and Figure S18). Moreover, the scattering profile is identical with the **UPy-UT-*g*-Si$_7$** bulk sample (*vide supra*, Figure 4C), concluding a similar packing on surface and in the bulk. The small particles, also visible on the AFM image, probably originate from disordered, aggregated material. Both elongated structures and particles were also observed in solution by scattering techniques (Figure S19).

The linear **UPy-UT-Si$_{16}$** only forms particles (Figure S17C), in contrast to UPy-UT containing main-chain supramolecular BCPs in the literature that mainly form fibers.[41,43,50] However, our results are in accordance with previously reported UPy-UT-functionalized PDMS which also did not form fibers, but undefined particles instead.[42] Hence, siloxane oligomers or polymers in the main chain prevent the UPy-UT from assembling into fibers in dilute solutions. Taken all together, these results show that a repetitive UPy-UT block in the main chain of **UPy-UT-*g*-Si$_7$** supramolecular polymers, grafted with *o*DMS, promotes the formation of exfoliated sheets in analogy to laterally grafted rod amphiphiles.[51,52]

Mechanical Properties of UPy-UT-Si$_{16}$ and UPy-UT-*g*-Si$_7$ Polymer Films. The association of the UPy-UT moiety in the oligomers allows for supramolecular polymerization to form polymeric materials which could be processed into thin films (Figure 7A,B). Hereto, the BCOs are dissolved in chloroform (~1 g mL^{-1}) and dropcasted into a Teflon mold, resulting in films with a thickness of 0.15 mm. Films of **UPy-UT-Si$_{16}$** are transparent and flexible while **UPy-UT-*g*-Si$_7$** films are opaque and very brittle. The stress−strain curve of **UPy-UT-*g*-Si$_7$** is indicative for a brittle material as only 1.7% strain could be reached at a ramp rate of 1 mm min^{-1} (Figure 7C). On the other hand, **UPy-UT-Si$_{16}$** is more ductile since a higher strain (12%) could be reached. Furthermore, the material can endure a higher stress, and therefore it is a better performing

https://dx.doi.org/10.1021/acs.macromol.0c02237
Macromolecules 2020, 53, 10289−10298

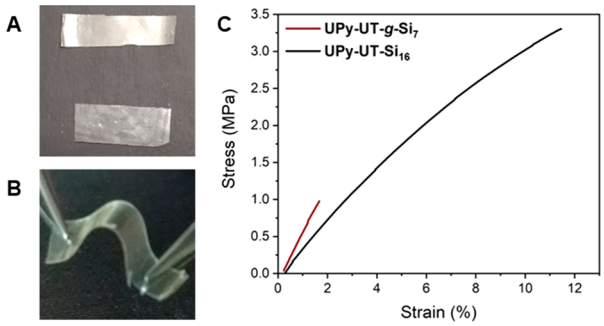

Figure 7. (A) Picture of films of **UPy-UT-*g*-Si$_7$** (left, top) and **UPy-UT-Si$_{16}$** (left, bottom) and (B) a bended film of **UPy-UT-Si$_{16}$** showing its flexibility. (C) True stress−strain curve of **UPy-UT-*g*-Si$_7$** (red) and **UPy-UT-Si$_{16}$** (black) measured at 1 mm min^{-1}, 0.15 mm thick films.

polymer than the grafted analogue. We attribute the higher extent of ductility in **UPy-UT-Si$_{16}$** to the alternating soft−hard block design in the main chain of the supramolecular BCP. Thus, upon application of a force on the sample, the stress is released by the *o*DMS midblock due to the coiled coil conformation of the amorphous oligomer. In contrast, the rigidity and crystallinity in the main chain of **UPy-UT-*g*-Si$_7$** supramolecular polymers prevent the release of stress. Upon application of a force, the stiff backbone bears most of the stress, and therefore the material breaks at low strain. These phenomena are in analogy to traditional ABA BCPs in which the midblock is usually an amorphous, rubbery polymer, yielding good mechanical properties.[53]

CONCLUSION

We successfully synthesized two types of discrete UPy-UT functionalized *o*DMS BCOs of which the molecular architecture differed from linear grafted structures. In general, the UPy-UT block crystallizes as a consequence of urethane hydrogen bonding in addition to UPy dimerization. The crystallization-driven assembly of the bulk material resulted in a lamellar morphology irrespective of the siloxane volume fraction and geometry of the BCO. However, the degree of crystallization was lower for the linear analogue compared to the grafted architecture. Hence, the competition between the amorphous, phase-segregated and crystalline states in the linear, alternating UPy-UT-*o*DMS BCPs results in less ordered and smaller crystalline domains in the lamellar morphology. In contrast, the BCO with *o*DMS grafts on the rigid supramolecular main chain is highly ordered due to a more stable and efficient crystalline packing. The grafted architecture allows for straightforward formation of micrometer-sized 2D sheets. For the mechanical properties, the grafted molecular architecture is disadvantageous as a very brittle material is obtained. The alternating structure of the soft and hard blocks in the linear BCO is beneficial for the polymer properties as it induces ductility in the material. From these results, we conclude that perfectly defined and long-range ordered nanoscale organization comes at the cost of bulk material properties, and therefore it remains a challenge for the future to obtain nanoscale ordered materials with excellent mechanical and physical properties.

With this study, we gained insight into the influence of the molecular structure on the nanostructure in semicrystalline, supramolecular BCP. We understand how the nanoscale morphology influences the macroscopic, material properties. Hence, the present work is a step forward toward the design of new and advanced (2D) polymeric materials by understanding the structure−property relationship from the molecular level to nanoscale and macroscopic properties.

ASSOCIATED CONTENT

Supporting Information

The Supporting Information is available free of charge at https://pubs.acs.org/doi/10.1021/acs.macromol.0c02237.

Experimental procedures, characterization data, and Figures S1−S19 (PDF)

AUTHOR INFORMATION

Corresponding Author

Ghislaine Vantomme − *Institute for Complex Molecular Systems and Laboratory of Macromolecular and Organic Chemistry, Eindhoven University of Technology, 5600 MB Eindhoven, The Netherlands;* orcid.org/0000-0003-2036-8892; Email: g.vantomme@tue.nl

Authors

Brigitte A. G. Lamers − *Institute for Complex Molecular Systems and Laboratory of Macromolecular and Organic Chemistry, Eindhoven University of Technology, 5600 MB Eindhoven, The Netherlands*

Joost J. B. van der Tol − *Institute for Complex Molecular Systems and Laboratory of Macromolecular and Organic Chemistry, Eindhoven University of Technology, 5600 MB Eindhoven, The Netherlands*

Kasper M. Vonk − *Institute for Complex Molecular Systems and Laboratory of Macromolecular and Organic Chemistry, Eindhoven University of Technology, 5600 MB Eindhoven, The Netherlands*

Bas F. M. de Waal − *Institute for Complex Molecular Systems and Laboratory of Macromolecular and Organic Chemistry, Eindhoven University of Technology, 5600 MB Eindhoven, The Netherlands*

Anja R. A. Palmans − *Institute for Complex Molecular Systems and Laboratory of Macromolecular and Organic Chemistry, Eindhoven University of Technology, 5600 MB Eindhoven, The Netherlands;* orcid.org/0000-0002-7201-1548

E. W. Meijer − *Institute for Complex Molecular Systems and Laboratory of Macromolecular and Organic Chemistry, Eindhoven University of Technology, 5600 MB Eindhoven, The Netherlands;* orcid.org/0000-0003-4126-7492

Complete contact information is available at: https://pubs.acs.org/10.1021/acs.macromol.0c02237

Author Contributions

⊥B.A.G.L. and J.J.B.v.d.T.: These authors contributed equally to this work.

Notes

The authors declare no competing financial interest.

ACKNOWLEDGMENTS

This work was financed by the Royal Netherlands Academy of Arts and Sciences and the Dutch Ministry of Education, Culture and Science (Gravity program 024.001.035) and NWO-VENI Grant 722.017.003.

REFERENCES

(1) Sakamoto, J.; Van Heijst, J.; Lukin, O.; Schlüter, A. D. Two-Dimensional Polymers: Just a Dream of Synthetic Chemists? *Angew. Chem., Int. Ed.* **2009**, *48* (6), 1030−1069.

(2) Zhuang, X.; Mai, Y.; Wu, D.; Zhang, F.; Feng, X. Two-Dimensional Soft Nanomaterials: A Fascinating World of Materials. *Adv. Mater.* **2015**, *27* (3), 403−427.

(3) Yang, F.; Cheng, S.; Zhang, X.; Ren, X.; Li, R.; Dong, H.; Hu, W. 2D Organic Materials for Optoelectronic Applications. *Adv. Mater.* **2018**, *30*, 1702415.

(4) Yang, J. C.; Mun, J.; Kwon, S. Y.; Park, S.; Bao, Z.; Park, S. Electronic Skin: Recent Progress and Future Prospects for Skin-Attachable Devices for Health Monitoring, Robotics, and Prosthetics. *Adv. Mater.* **2019**, *31* (48), 1970337.

(5) Yan, C.; Barlow, S.; Wang, Z.; Yan, H.; Jen, A. K. Y.; Marder, S. R.; Zhan, X. Non-Fullerene Acceptors for Organic Solar Cells. *Nat. Rev. Mater.* **2018**, *3*, 1−19.

(6) Lessard, J. J.; Scheutz, G. M.; Sung, S. H.; Lantz, K. A.; Epps, T. H.; Sumerlin, B. S. Block Copolymer Vitrimers. *J. Am. Chem. Soc.* **2020**, *142*, 283−289.

(7) Bates, C. M.; Bates, F. S. 50th Anniversary Perspective: Block Polymers-Pure Potential. *Macromolecules* **2017**, *50* (1), 3−22.

(8) Bates, F.; Fredrickson, G. H. Block Copolymer Thermodynamics: Theory And Experiment. *Annu. Rev. Phys. Chem.* **1990**, *41* (1), 525−557.

(9) Leibler, L. Theory of Microphase Separation in Block Copolymers. *Macromolecules* **1980**, *13* (10), 1602−1617.

(10) Bates, F. S.; Hillmyer, M. A.; Lodge, T. P.; Bates, C. M.; Delaney, K. T.; Fredrickson, G. H. Multiblock Polymers: Panacea or Pandora's Box? *Science* **2012**, *336*, 434−440.

(11) Feng, H.; Lu, X.; Wang, W.; Kang, N. G.; Mays, J. W. Block Copolymers: Synthesis, Self-Assembly, and Applications. *Polymers (Basel, Switz.)* **2017**, *9* (10), 494.

(12) Gentekos, D. T.; Fors, B. P. Molecular Weight Distribution Shape as a Versatile Approach to Tailoring Block Copolymer Phase Behavior. *ACS Macro Lett.* **2018**, *7* (6), 677−682.

(13) Sinturel, C.; Bates, F. S.; Hillmyer, M. A. High χ-Low N Block Polymers: How Far Can We Go? *ACS Macro Lett.* **2015**, *4* (9), 1044−1050.

(14) Matsen, M. W. Effect of Architecture on the Phase Behavior of AB-Type Block Copolymer Melts. *Macromolecules* **2012**, *45* (4), 2161−2165.

(15) Bates, F. S.; Fredrickson, G. H. Block Copolymers-Designer Soft Materials. *Phys. Today* **1999**, *52* (2), 32−38.

(16) Matyjaszewski, K. Architecturally Complex Polymers with Controlled Heterogeneity. *Science* **2011**, *333* (6046), 1104−1105.

(17) Karavolias, M. G.; Elder, J. B.; Ness, E. M.; Mahanthappa, M. K. Order-to-Disorder Transitions in Lamellar Melt Self-Assembled Core − Shell Bottlebrush Polymers. *ACS Macro Lett.* **2019**, *8*, 1617−1622.

(18) Wei, Y.; Li, B.; Han, Y.; Pan, C. Ring-Shaped Morphology in H-Shaped Block Copolymer Thin Films. *Soft Matter* **2008**, *4* (12), 2507−2512.

(19) Pitet, L. M.; Chamberlain, B. M.; Hauser, A. W.; Hillmyer, M. A. Dispersity and Architecture Driven Self-Assembly and Confined Crystallization of Symmetric Branched Block Copolymers. *Polym. Chem.* **2019**, *10* (39), 5385−5395.

(20) Gido, S. P.; Lee, C.; Pochan, D. J.; Pispas, S.; Mays, J. W.; Hadjichristidis, N. Synthesis, Characterization, and Morphology of Model Graft Copolymers with Trifunctional Branch Points. *Macromolecules* **1996**, *29* (22), 7022−7028.

(21) Shi, W.; Tateishi, Y.; Li, W.; Hawker, C. J.; Fredrickson, G. H.; Kramer, E. J. Producing Small Domain Features Using Miktoarm Block Copolymers with Large Interaction Parameters. *ACS Macro Lett.* **2015**, *4* (11), 1287−1292.

(22) Hirao, A.; Murano, K.; Oie, T.; Uematsu, M.; Goseki, R.; Matsuo, Y. Chain-End- and in-Chain-Functionalized AB Diblock Copolymers as Key Building Blocks in the Synthesis of Well-Defined Architectural Polymers. *Polym. Chem.* **2011**, *2* (6), 1219−1233.

(23) Isono, T.; Kawakami, N.; Watanabe, K.; Yoshida, K.; Otsuka, I.; Mamiya, H.; Ito, H.; Yamamoto, T.; Tajima, K.; Borsali, R.; et al. Microphase Separation of Carbohydrate-Based Star-Block Copolymers with Sub-10 Nm Periodicity. *Polym. Chem.* **2019**, *10*, 1119−1129.

(24) Ruzette, A.-V.; Leibler, L. Block Copolymers in Tomorrow's Plastics. *Nat. Mater.* **2005**, *4*, 19−31.

(25) Van Genabeek, B.; de Waal, B. F. M.; Gosens, M. M. J.; Pitet, L. M.; Palmans, A. R. A.; Meijer, E. W. Synthesis and Self-Assembly of Discrete Dimethylsiloxane−Lactic Acid Diblock Co-Oligomers: The Dononacontamer and Its Shorter Homologues. *J. Am. Chem. Soc.* **2016**, *138* (12), 4210−4218.

(26) Oschmann, B.; Lawrence, J.; Schulze, M. W.; Ren, J. M.; Anastasaki, A.; Luo, Y.; Nothling, M. D.; Pester, C. W.; Delaney, K. T.; Connal, L. A.; et al. Effects of Tailored Dispersity on the Self-Assembly of Dimethylsiloxane-Methyl Methacrylate Block Co-Oligomers. *ACS Macro Lett.* **2017**, *6* (7), 668−673.

(27) Zhang, C.; Bates, M. W.; Geng, Z.; Levi, A. E.; Vigil, D.; Barbon, S. M.; Loman, T.; Delaney, K. T.; Fredrickson, G. H.; Bates, C. M.; Whittaker, A. K.; Hawker, C. J. Rapid Generation of Block Copolymer Libraries Using Automated Chromatographic Separation. *J. Am. Chem. Soc.* **2020**, *142* (21), 9843−9849.

(28) Lamers, B. A. G.; van Genabeek, B.; Hennissen, J.; de Waal, B. F. M.; Palmans, A. R. A.; Meijer, E. W. Stereocomplexes of Discrete, Isotactic Lactic Acid Oligomers Conjugated with Oligodimethylsiloxanes. *Macromolecules* **2019**, *52* (3), 1200−1209.

(29) Van Genabeek, B.; de Waal, B. F. M.; Palmans, A. R. A.; Meijer, E. W. Discrete Oligodimethylsiloxane-Oligomethylene Di- and Triblock Co-Oligomers: Synthesis and Self-Assembly and Molecular Organization. *Polym. Chem.* **2018**, *9* (20), 2746−2758.

(30) Yang, W.; Zhang, W.; Luo, L.; Lyu, X.; Xiao, A.; Shen, Z.; Fan, X.-H. Ordered Structures and Sub-5 Nm Line Patterns from Rod−coil Hybrids Containing Oligo(dimethylsiloxane). *Chem. Commun.* **2020**, *56*, 10341−10344.

(31) Zha, R. H.; Vantomme, G.; Berrocal, J. A.; Gosens, R.; de Waal, B. F. M.; Meskers, S.; Meijer, E. W. Photoswitchable Nanomaterials Based on Hierarchically Organized Siloxane Oligomers. *Adv. Funct. Mater.* **2018**, *28* (1), 1703952.

(32) Berrocal, J. A.; Zha, R. H.; de Waal, B. F. M.; Lugger, J. A. M.; Lutz, M.; Meijer, E. W. Unraveling the Driving Forces in the Self-Assembly of Monodisperse Naphthalenediimide-Oligodimethylsiloxane Block Molecules. *ACS Nano* **2017**, *11* (4), 3733−3741.

(33) Zha, R. H.; De Waal, B. F. M.; Lutz, M.; Teunissen, A. J. P.; Meijer, E. W. End Groups of Functionalized Siloxane Oligomers Direct Block-Copolymeric or Liquid-Crystalline Self-Assembly Behavior. *J. Am. Chem. Soc.* **2016**, *138* (17), 5693−5698.

(34) Yang, S. K.; Ambade, A. V.; Weck, M. Main-Chain Supramolecular Block Copolymers. *Chem. Soc. Rev.* **2011**, *40*, 129−137.

(35) Hirschberg, J. H. K. K.; Beijer, F. H.; Van Aert, H. A.; Magusin, P. C. M. M.; Sijbesma, R. P.; Meijer, E. W. Supramolecular Polymers from Linear Telechelic Siloxanes with Quadruple-Hydrogen-Bonded Units. *Macromolecules* **1999**, *32* (8), 2696−2705.

(36) Voorhaar, L.; Hoogenboom, R. Supramolecular Polymer Networks: Hydrogels and Bulk Materials. *Chem. Soc. Rev.* **2016**, *45* (14), 4013−4031.

(37) Weng, W.; Li, Z.; Jamieson, A. M.; Rowan, S. J. Control of Gel Morphology and Properties of a Class of Metallo-Supramolecular Polymers by Good/Poor Solvent Environments. *Macromolecules* **2009**, *42* (1), 236−246.

(38) Cortese, J.; Soulié-Ziakovic, C.; Cloitre, M.; Tencé-Girault, S.; Leibler, L. Order-Disorder Transition in Supramolecular Polymers. *J. Am. Chem. Soc.* **2011**, *133* (49), 19672−19675.

(39) Fox, J. D.; Rowan, S. J. Supramolecular Polymerizations and Main-Chain Supramolecular Polymers. *Macromolecules* **2009**, *42* (18), 6823−6835.

(40) Sijbesma, R. P.; Beijer, F. H.; Brunsveld, L.; Folmer, B. J. B.; Hirschberg, J. H. K. K.; Lange, R. F. M.; Lowe, J. K. L.; Meijer, E. W. Reversible Polymers Formed from Self-Complementary Monomers

https://dx.doi.org/10.1021/acs.macromol.0c02237
Macromolecules 2020, 53, 10289−10298

Using Quadruple Hydrogen Bonding. *Science* **1997**, *278* (5343), 1601−1604.
(41) Kautz, H.; Van Beek, D. J. M.; Sijbesma, R. P.; Meijer, E. W. Cooperative End-to-End and Lateral Hydrogen-Bonding Motifs in Supramolecular Thermoplastic Elastomers. *Macromolecules* **2006**, *39* (13), 4265−4267.
(42) Botterhuis, N. E.; van Beek, D. J. M.; van Gemert, G. M. L.; Bosman, A. W.; Sijbesma, R. P. Self-Assembly and Morphology of Polydimethylsiloxane Supramolecular Thermoplastic Elastomers. *J. Polym. Sci., Part A: Polym. Chem.* **2008**, *46*, 3877−3885.
(43) Van Beek, D. J. M.; Spiering, A. J. H.; Peters, G. W. M.; Te Nijenhuis, K.; Sijbesma, R. P. Unidirectional Dimerization and Stacking of Ureidopyrimidinone End Groups in Polycaprolactone Supramolecular Polymers. *Macromolecules* **2007**, *40* (23), 8464−8475.
(44) Van Horn, R. M.; Steffen, M. R.; O'Connor, D. Recent Progress in Block Copolymer Crystallization. *Polym. Cryst.* **2018**, *1* (4), 1−46.
(45) Wang, H.; Lu, W.; Wang, W.; Shah, P. N.; Misichronis, K.; Kang, N. G.; Mays, J. W. Design and Synthesis of Multigraft Copolymer Thermoplastic Elastomers: Superelastomers. *Macromol. Chem. Phys.* **2018**, *219* (1), 1700254.
(46) Zhang, J.; Li, T.; Mannion, A. M.; Schneiderman, D. K.; Hillmyer, M. A.; Bates, F. S. Tough and Sustainable Graft Block Copolymer Thermoplastics. *ACS Macro Lett.* **2016**, *5* (3), 407−412.
(47) Lynd, N. A.; Oyerokun, F. T.; O'Donoghue, D. L.; Handlin, D. L.; Fredrickson, G. H. Design of Soft and Strong Thermoplastic Elastomers Based on Nonlinear Block Copolymer Architectures Using Self-Consistent-Field Theory. *Macromolecules* **2010**, *43* (7), 3479−3486.
(48) Beijer, F. H.; Sijbesma, R. P.; Kooijman, H.; Spek, A. L.; Meijer, E. W. Strong Dimerization of Ureidopyrimidones via Quadruple Hydrogen Bonding. *J. Am. Chem. Soc.* **1998**, *120* (27), 6761−6769.
(49) Dong, R.; Zhang, T.; Feng, X. Interface-Assisted Synthesis of 2D Materials: Trend and Challenges. *Chem. Rev.* **2018**, *118*, 6189−6235.
(50) Appel, W. P. J.; Portale, G.; Wisse, E.; Dankers, P. Y. W.; Meijer, E. W. Aggregation of Ureido-Pyrimidinone Supramolecular Thermoplastic Elastomers into Nanofibers: A Kinetic Analysis. *Macromolecules* **2011**, *44* (17), 6776−6784.
(51) Shin, S.; Lim, S.; Kim, Y.; Kim, T.; Choi, T. L.; Lee, M. Supramolecular Switching between Flat Sheets and Helical Tubules Triggered by Coordination Interaction. *J. Am. Chem. Soc.* **2013**, *135* (6), 2156−2159.
(52) Lee, E.; Kim, J. K.; Lee, M. Reversible Scrolling of Two-Dimensional Sheets from the Self-Assembly of Laterally Grafted Amphiphilic Rods. *Angew. Chem., Int. Ed.* **2009**, *48* (20), 3657−3660.
(53) Koo, C. M.; Wu, L.; Lim, L. S.; Mahanthappa, M. K.; Hillmyer, M. A.; Bates, F. S. Microstructure and Mechanical Properties of Semicrystalline-Rubbery-Semicrystalline Triblock Copolymers. *Macromolecules* **2005**, *38* (14), 6090−6098.

https://dx.doi.org/10.1021/acs.macromol.0c02237
Macromolecules 2020, 53, 10289−10298